New Journal of Physics
The open access journal at the forefront of physics

Deutsche Physikalische Gesellschaft DPG
IOP Institute of Physics

Published in partnership with: Deutsche Physikalische Gesellschaft and the Institute of Physics

OPEN ACCESS

RECEIVED
3 April 2020

REVISED
22 June 2020

ACCEPTED FOR PUBLICATION
8 July 2020

PUBLISHED
17 August 2020

PAPER

Wigner function and photon number distribution of a superradiant state in semiconductor heterostructures

Peter P Vasil'ev[1,2] **and Richard V Penty**[1]

[1] Centre for Photonic Systems, University of Cambridge, 9 JJ Thomson Avenue, Cambridge, CB3 0FA, United Kingdom
[2] Quantum Radiophysics Department, PN Lebedev Physical Institute, 53 Leninsky Prospect, Moscow 119991, Russia

E-mail: pv261@cam.ac.uk

Keywords: superradiance, Wigner function, homodyne tomography, displaced Fock state

Abstract

Advanced quantum technologies require sources of non-Gaussian and non-classical light. For the understanding of properties of quantum light it is necessary to reconstruct its quantum state. Here, we use time-domain optical homodyne tomography for the quantum state recognition and reconstruction of the femtosecond optical field from a nonequilibrium superradiant coherent electron–hole state formed in a semiconductor GaAs/AlGaAs heterostructure. We observe severe deviations from the Poissonian statistics of the photons associated with the coherent state when the transformation from lasing to superradiance occurs. The estimated Mandel parameter Q of the superradiant states is in the range of 1.08–1.89. The reconstructed Wigner functions show large areas of negative values, a characteristic sign of non-classicality, demonstrating the quantum nature of the generated superradiant emission. The photon number distribution and Wigner function of the superradiant state are very similar to those of the displaced Fock state.

1. Introduction

Recent advances in the field of quantum optics have paved a way to technologies based on quantum properties of light, including quantum communications, quantum cryptography and computation [1, 2]. In contrast to classical optics, quantum optics has enabled those approaches using principles based on laws of quantum mechanics. The approaches and experimental techniques developed in quantum optics allow for investigating a number of unique phenomena such as entanglement and teleportation and studying different quantum states of field and matter, including coherent, squeezed, and Schrödinger-cat states [3].

Nonclassical light has been attracting particular attention in quantum optics over the last two decades. The features of nonclassical light include squeezing, [4], oscillatory photon statistics [5], sub- and super-Poissonian statistics [6], photon antibunching [7] and entanglement [8]. It has been shown that squeezing as well as sub-Poissonian photon statistics [9] and oscillations of the photon number distribution [10], can emerge from a superposition of coherent states. In addition, mutually independent coherent excitations is at the essence of super-Poissonian chaotic light states [11]. Nonclassicality is also a feature of displaced Fock (number) states (DFS), which are considered as non-classical generalizations of coherent states [12]. The photon number distribution of DFS has been shown to display oscillations, which are interpreted as interference in phase space [13].

It has been a long discussion in the literature concerning the connection between entanglement in many-body systems and quantum phase transition, in particular, superradiant (SR) phase transition. Initial indications suggested that entanglement may not be a feature of the idealized Dicke model superradiance, despite its exemplification of many-body effects [14]. The relation between entangled states and SR phase transitions was studied by Aparicio Alcalde *et al* [15]. It was found that the dipole–dipole interaction between atoms was able to generate entangled states in the atomic system. A review of recent developments on entanglement and nonclassical effects in collective two-atom systems and a uniform physical picture of

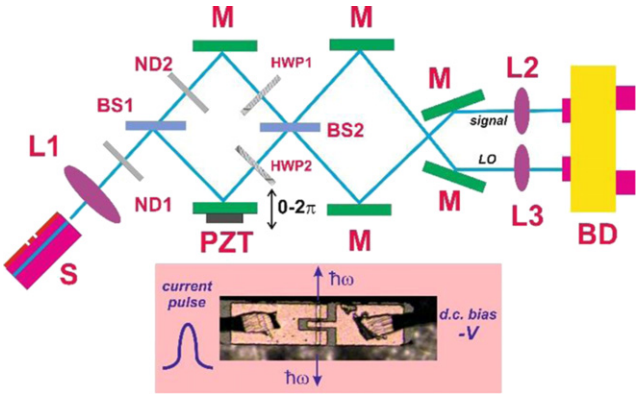

Figure 1. Experimental setup. S is a sample, L1, L2, and L3—lenses, ND1, 2—neutral density filters, BS1 and BS2—non-polarizing beam splitters, HWP1, 2—half-wave plates; M—mirrors, PZT—piezoelectric translator, BD—balanced photodetector. Inset: the microscopic top view of the sample with a 3-section design. The nanosecond current pulses are applied on the left electrode, the right section is reverse biased by a dc voltage. The output light is emitted in opposite directions.

the many predicted related phenomena can be found elsewhere [16]. It should be pointed out that the non-classicality of atom states and emitted photon states are two completely different subjects. One does not yet automatically assume the other. Superbunching and nonclassicality as new hallmarks of superradiance were discussed by Bhatti *et al* [17]. They investigated whether it was possible to obtain nonclassical light, a sub-Poissonian photon statistics, and antibunching in two-photon superradiance.

Superradiance and generalized Dicke model [18] has recently attracted an enhanced interest both in quantum optics and electrodynamics. Indeed, this model is a fairly simple system where entanglement and related phenomena can be found. Furthermore, the superradiant quantum phase transition was found to be relevant to quantum computing and quantum information [19–21]. SR emission has been generated from many types of media, including quantum dots at cryogenic temperatures [22]. We have previously reported the observation of the SR phase transition in 2D and 3D semiconductor laser devices with different material compositions at room temperature [23–26]. The observed SR emission exhibited many remarkable features, including stronger coherence than lasing, superluminal propagation and ultrabright internal second-harmonic generation. The physical reason behind these effects consists in the quantum phase transition and non-equilibrium condensation of electrons and holes in phase space which occurs in the semiconductor [27, 28]. However, the quantum features of SR states in semiconductors have not been investigated.

For the visualization of quantum states, the approach based on Wigner functions has been widely used for a long time [29–31]. This representation reveals amazing properties of different classical or quantum states, for example, the oscillatory photon statistics or negative values of Wigner functions. Moreover, the approach provides a possibility of reconstructing quantum states using optical homodyne tomography [32].

In this paper, we determine the density matrix, the photon number distribution and reconstruct the Wigner function of SR light emitted due to radiative recombination of the coherent e–h BCS-like collective state using optical quantum-state tomography exploiting homodyne detection.

2. Methods

A set of GaAs/AlGaAs bulk heterostructures capable of generating SR emission have been studied. Each device has a gain-absorber–gain geometry with different gain/absorber ratios and total cavity lengths between 90 and 250 microns. The parameters of the devices were described in detail in our previous publications [24–26]. The content of Al of the GaAs/AlGaAs heterostructures was varied, which resulted in a broad range of operating wavelengths in the range of 810–890 nm. Depending on the driving conditions, the samples operated under continuous-wave or SR regimes. Figure 1 shows the experimental set-up. The emission from a sample is collimated by a diode lens with an NA of 0.5 and is fed into an interferometer consisting of two non-polarizing beam splitters. The input beam is attenuated by step and variable neutral density filters with different optical densities depending on the required signal level on the detector. One mirror is attached to a piezoelectric translator and placed on a precise translation stage. The interferometer is aligned to provide a zero difference of the optical paths of both arms. The two beams from the interferometer are focused on the two inputs of a balanced photodetector. The homodyne photocurrent is recorded by a 300 MHz digital oscilloscope with a sampling rate of up to 4 G samples/s.

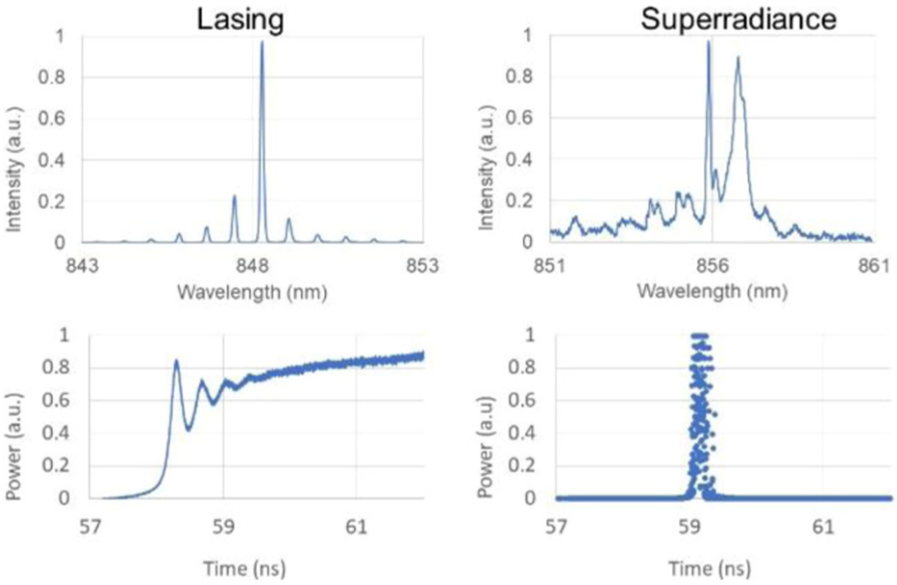

Figure 2. Optical spectra and output waveform as detected by a high-speed photodiode and sampling oscilloscope of lasing and SR emission from the same device.

The digitized data is numerically integrated over time intervals equal to the width of the pulses detected by the balanced detector. Each integral corresponded a single quadrature measurement. This method is used as a standard in pulsed homodyne detection using mode-locked solid-state and pulsed semiconductor laser sources [33, 34]. Each homodyne trace consists of 10^6 experimental data. The measured transmission/reflection ratio of the interferometer beam splitter is 0.52:0.48 in the wavelength range of 840–870 nm. Rotation of the half-wave plate allows us to adjust the splitting ratio of the beam splitter. The total apparatus efficiency η (represents the proportion of photons which are not detected due to the losses in the measurement process) is around 0.38. It has been previously shown that the presence of low detection efficiency (<50%) does not prevent the tomographic reconstruction of quantum states of light [34]. Even quantum interferences of two coherent states can be effectively reconstructed by experimental set-ups with low homodyne detection efficiency [35].

The experimental set-up is first tested for quantum state reconstruction using two single-mode c.w. and pulsed semiconductor lasers operating at 652 and 778 nm. The density matrix and Wigner functions are reconstructed for cases with different numbers of photons per mode. The test results provided standard coherent laser states with Poissonian statistics of photons as expected.

3. Results

When current pulses are applied on both contacts of a heterostructure simultaneously, the standard laser emission is generated. The lasing threshold is typically below 100 mA. The optical spectrum and the output light pulse are shown in figure 2 (left). The output optical pulse exhibits some typical relaxation oscillations. Strictly speaking, it is lasing that prevents the onset of SR phase transition which requires much larger e–h densities [23]. A strong reverse bias of the absorber section is used for the elimination of the onset of lasing for a long enough time. That allows for achieving much larger e–h densities due to continuous pumping of the gain sections. When SR phase transition occurs in the system at the critical density, giant femtosecond pulses are emitted as a result of a cooperative radiative decay of the e–h ensemble [23, 27]. The overall SR photon number emitted from the heterostructure is typically in the range of 10^7–10^8 which is well above the saturated power of the photodetector. The ND filters (see figure 1) reduce hugely the light intensity to have the recorded mean photon number per pulse of less than 20–30. This limits the sizes of the reconstructed density matrix ($<60 \times 60$) and Wigner functions. Larger mean photon numbers require much longer calculation times for the reconstruction and result in enhanced errors of the calculation.

The SR optical spectrum consists of a doublet, the emission peak being red-shifted by about 8 nm with respect to the lasing wavelength (figure 2). The separation of the components of the doublet exceeds by over 10% the spacing of the laser modes, which corresponds to a decrease of the group refractive index during SR [25]. The femtosecond SR pulse exhibits a huge jitter (phase fluctuations) which is common to all SR

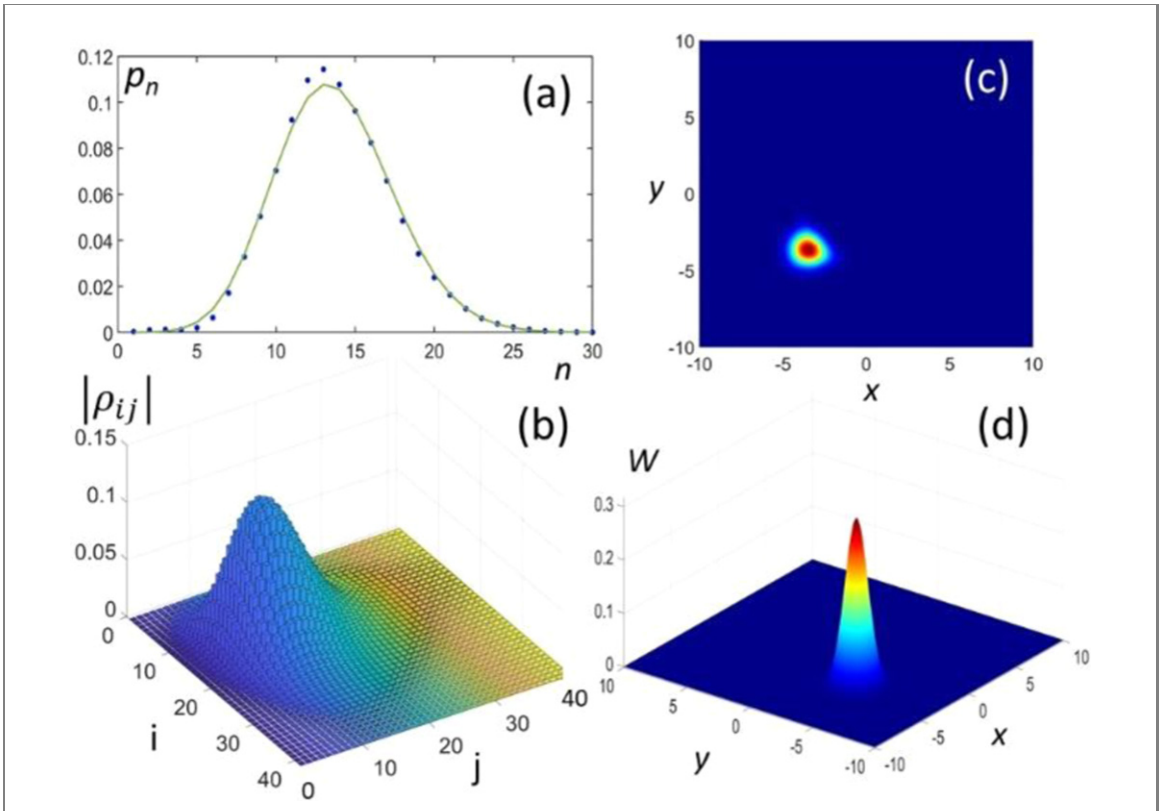

Figure 3. The reconstruction of the coherent laser state. (a) Photon number distribution p_n. The dots correspond to the measured data. The green line presents the Poissonian statistics of the photons, (b) 3D plot of the absolute values of the density matrix elements $|\rho_{ij}|$, (d) the reconstructed Wigner function and (c) its 2D projection.

pulses [36]. If the duration of the current pulses is longer than approximately 8–9 ns, a number of SR pulses is generated instead of a single pulse. Each pulse is individual because all SR pulses originate from spontaneous noise. For the matter of purity, quantum state reconstruction is performed for cases of single SR pulses.

Figure 3 presents the results of the reconstruction of the coherent laser state at a certain current amplitude above the lasing threshold, when the nanosecond current pulses are applied to both device sections. This causes the uniform current injection without any saturable absorption in the sample. The homodyne traces are measured for the relative delay range corresponding to the central interference optical cycle. The optical spectrum and output light pulse are shown in figure 2. The spectrum consists of a main mode with a few low-intensity side modes. The coherence time of the laser emission is around 30 ps which is much smaller than the current pulse duration.

The green line in figure 3(a) shows the Poissonian statistics of the photons which is given by

$$p_n = \frac{\langle n \rangle^n}{n!} \mathrm{e}^{-\langle n \rangle} \tag{1}$$

with $\langle n \rangle$ being the mean photon number. For the given experimental situation, we obviously have a coherent laser state obeying the Poissonian statistics with $\langle n \rangle \sim 13$. The experimental data allows for estimating the second-order correlation function $g^{(2)}(0)$

$$g^{(2)}(0) = \frac{\langle n^2 \rangle - \langle n \rangle}{\langle n \rangle^2}. \tag{2}$$

The experimental value of $g^{(2)}(0)$ in figure 3 is 0.998, which is very close to the theoretical value of 1.0 for a coherent state.

Figures 4 and 5 present the results of the reconstruction of the SR states at different current amplitudes I and reverse biases V on the saturable absorber.

In contrast to the coherent laser state (figure 3), all SR states exhibit severe deviations of the photon statistics from the Poissonian statistics and significant areas where the Wigner functions have negative values. This amazing feature makes it impossible to treat the Wigner function as a correct probability distribution. The photon number distribution in figures 4(a) and 5(a) has 2 peaks which are particularly

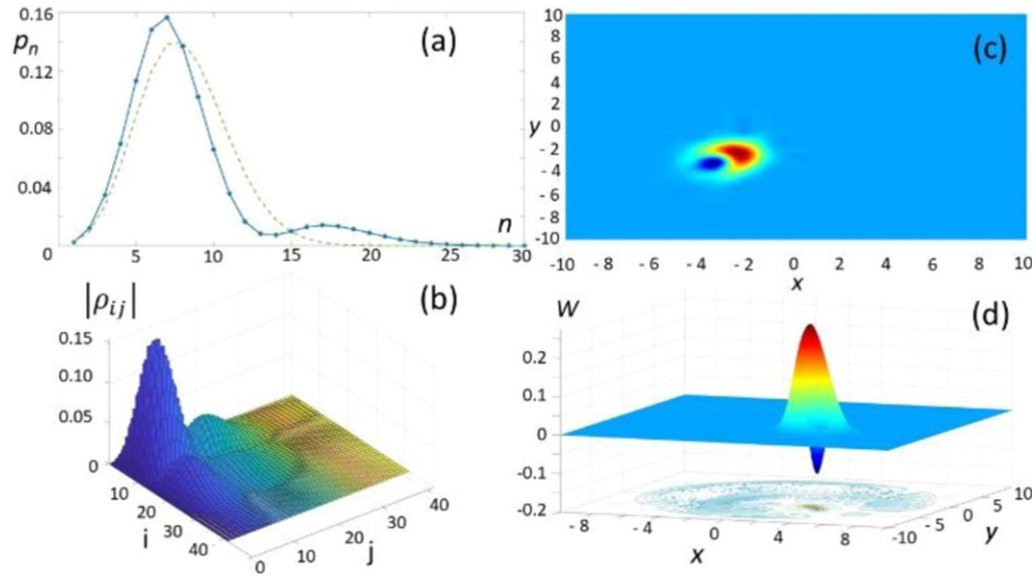

Figure 4. The reconstruction of the SR state at $I = 410$ mA and $V = -4.1$ V. (a) Photon number distribution p_n. The dots and blue line correspond to the measured data. The green dashed line presents the Poissonian statistics of photons of a coherent state, (b) 3D plot of the absolute values of the density matrix elements $|\rho_{ij}|$, (c) 2D projection of the reconstructed 3D Wigner function (d).

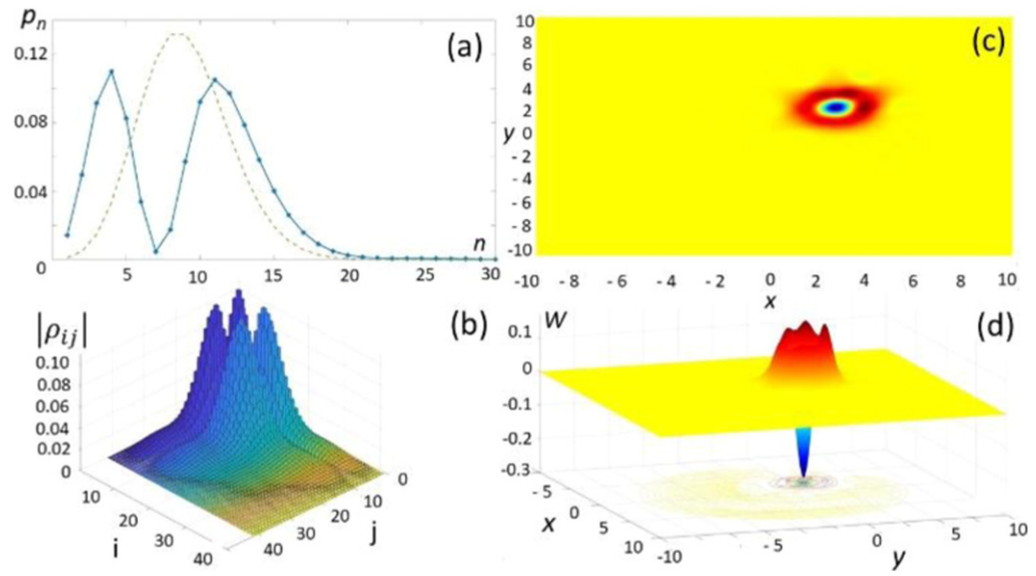

Figure 5. The reconstruction of the SR state at $I = 630$ mA and $V = -6.7$ V. (a) Photon number distribution p_n. The dots and blue line correspond to the measured data. The green dashed line presents the Poissonian statistics of photons of a coherent state, (b) 3D plot of the absolute values of the density matrix elements $|\rho_{ij}|$, (c) 2D projection of the reconstructed 3D Wigner function (d).

visible in the last case. The experimental values of $g^{(2)}(0)$ are 1.14, 1.17 and 1.19 for the data in figures 4–6, respectively. The Mandel parameter Q [37] of the SR states

$$Q = \frac{\left\langle (\Delta n)^2 \right\rangle - \langle n \rangle}{\langle n \rangle} \tag{3}$$

are in the range of 1.08–1.89. This means that the SR states have super-Poissonian statistics. The experimental value of the parameter Q for the coherent state shown in figure 3 is −0.02 which is very close to the theoretical value 0.

The observed transformation of the photon statistics and Wigner functions from lasing to SR was abrupt.

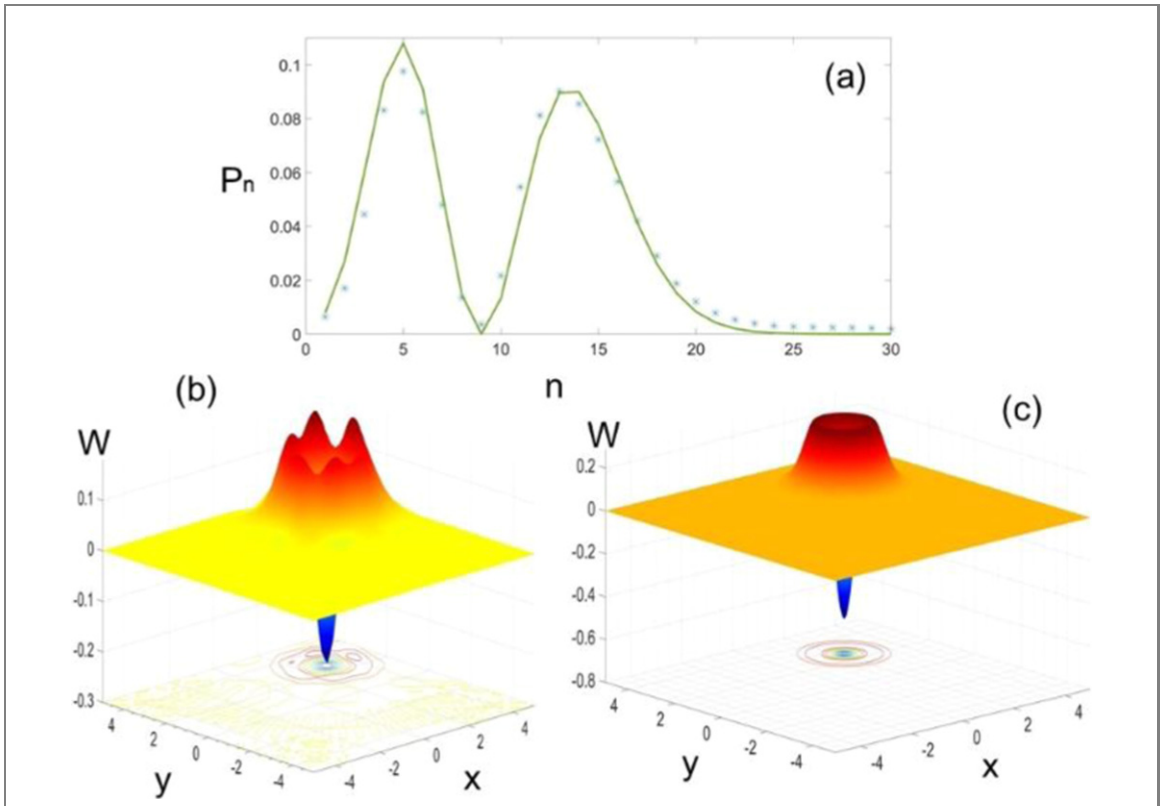

Figure 6. Comparison of the parameters of the measured SR state generated at $I = 770$ mA and V $= -7.2$ V and the calculated DFS $|\alpha, k = 1\rangle$. (a) The photon number distribution. The blue stars represent the SR state, the green line corresponds to the DFS with $|\alpha|^2 = 9$; (b) the reconstructed Wigner function of the SR state; (c) the calculated Wigner function of the DFS with $\alpha = 2.15 + 2.1^{*}i$.

Similar results were obtained with a number of the SR devices. The reproducibility of the measurement is very good and the relative experimental error is around 2%–3%. Further increase of the driving current amplitude above around 800 mA or the value of the reverse bias below -9 V resulted in a catastrophic degradation of the samples. That happened due to either an electrical discharge in the gaps between the upper metal electrodes (see figure 1) or an optical breakdown of the facets of the samples by the ultrahigh power flux density of the femtosecond SR pulses [38].

4. Discussion

In contrast to lasing, when the optical field is coherent and the active medium is incoherent, the feature of SR is that a non-equilibrium coherent BCS-like state is formed, e–h pairs being collectively paired like in an ensemble of Cooper pairs [23]. One can expect that quantum coherence of this state is translated to the electromagnetic field of the emitted light. The oscillatory behaviour of the photon number distributions and the specific shapes of the Wigner functions in figures 4 and 5 suggest the observation of quantum interference between coherent states [12]. Quantum interference in phase space is associated with off-diagonal matrix elements of quantum states. The quantum interference results, in particular, in oscillation behaviour of the photon number distribution.

One can see that both photon number distribution and the Wigner function of the SR state shown in figure 5 have specific shapes which bear a resemblance to those of a displaced number state, which is often called a DFS [12, 13, 39]. DFS are non-classical generalizations of coherent states. The DFS provides a clear illustration of the concept of interference in phase space. The photon number distribution of a DFS $|\alpha, k\rangle$ is given [12]

$$p_n^{(\alpha,k)} = \frac{\mathrm{e}^{-|\alpha|^2}|\alpha|^{2(n-k)}}{n!k!}\left|\sum_{m=0}^{k}\frac{n!k!(-1)^m|\alpha|^{2(k-m)}}{m!\,(k-m)!\,(n-m)!}\right|^2. \tag{4}$$

The Wigner function of the DFS is equal to the shifted Wigner function of the Fock state $|\alpha, k\rangle$ [12]

$$W_k^{(\alpha)}(\beta) = \frac{2(-1)^k}{\pi}\mathrm{e}^{(-2|\beta-\alpha|)^2}L_k(4|\beta-\alpha|^2). \tag{5}$$

where $L_k(x)$ is the Laguerre polynomial of order k. Let us consider a special case of $k = 1$. According to equation (4), the function $p_n^{(\alpha,1)}$ of the DFS is equal to 0 for $n = |\alpha|^2$. This is opposite to a coherent state for which the photon number distribution reaches the maximum value at $n = |\alpha|^2$.

Compare now the reconstructed SR state with the DFS $|\alpha, k = 1\rangle$. Figure 6 presents the characteristics of the SR state generated in one of the samples at $I = 770$ mA and $V = -7.2$ V and the photon number distribution and the Wigner function of the DFS calculated using equations (4) and (5). We use the notation $x = \mathrm{Re}\ \beta$ and $y = \mathrm{Im}\ \beta$. The photon number distribution of the SR state has a minimum value at $n = 9$. The calculated photon number distribution of the DFS fits very well to the experimental data for $|\alpha|^2 = 9$ (see figure 5(a)). The calculated Wigner function of the DFS looks a lot like the experimental one of the SR state. The latter is a bit broader than the former. The value of the negative peak of the Wigner function of the SR state is also smaller than that of the DFS. This may be caused by the fact that the calculations according to equation (4) do not take into account the damping and dissipation which are always present in real systems. Another reason may be determined by the ultrashort lifetime of the SR state under study.

To assess the similarity between the reconstructed quantum state with the Wigner function $W_{\mathrm{exp}}(\beta)$, and the assumed DFS, with Wigner function $W_k^{(\alpha)}(\beta)$ of equation (5), we use the parameter fidelity F as a figure of merit [40]. This quantity is essentially represented by the overlap between the Wigner functions for the two quantum states. Its value is in the range of $0 \leqslant F \leqslant 1$, reaching the unity when the two states obviously coincide. The quantity F is given by [8]

$$F = \pi \iint W_{\mathrm{exp}} W_k^{(\alpha)} \mathrm{d}x\, \mathrm{d}y. \tag{6}$$

The experimental value of F is 0.89 for a coherent state with $\langle n \rangle = 13$ and the reconstructed state in figure 3. The approximation of the experimental SR state in figure 6(b) by the DFS $|\alpha, 1\rangle$ (figure 6(c)) gives $F = 0.72$. The relatively small value of the fidelity means that the DFS $|\alpha, 1\rangle$ described by equation (5) does not fit exactly the experimental SR state. This may be because equation (5) does not take into account dissipation of the quantum state. Indeed, it has been shown [41, 42] that dissipation results in the loss of nonclassicality and non-Gaussianity of quantum states. In particular, dissipation suppresses phase–space interference between the states and oscillations of the photon number statistics. It also leads to the loss of negativities of Wigner functions and restoration of classical effects [42]. This can be seen in figures 6(b) and (c) where the maximum positive values of the Wigner functions are similar, but the minimum negative values differ a lot (-0.29 in figure 6(b) and -0.67 in figure 6(c)).

We observed SR states in some devices at harder pumping with the reconstructed photon number distributions and Wigner functions which were very similar to those of the DFS $|\alpha, k\rangle$ with $k > 1$. The 'tuning' of SR state with respect to the displaced number k can be done by variations of the driving current amplitude I or by the reverse bias V. It should be noted that both reconstructed Wigner functions and the photon number distributions of SR states are very sensitive to variations of I and V.

It should be noted that a superposition of coherent states can exhibit nonclassical behaviour which is similar to that of the observed SR states. That includes oscillations of the photon number distribution and negative values of the Wigner function [10]. However, the character of the oscillations is different from the experimentally observed ones. The shape of the Wigner function is also different. The additional results of our study showing that the SR states are closer to DFS than to a superposition of coherent states will be presented in the forthcoming publication.

5. Conclusion

In conclusion, we have experimentally demonstrated that quantum light can be generated from semiconductor heterostructures during the SR phase transition. Using a time-domain optical homodyne tomography we have performed quantum state recognition and the reconstruction of the optical field from a nonequilibrium superradiant coherent electron–hole state. We have observed the oscillatory behaviour and severe deviations from the Poissonian statistics of the photons. The estimated Mandel parameter Q of the SR states is in the range of 1.08–1.89. We interpret the photon distribution oscillations as the result of quantum interference in phase space. The reconstructed Wigner functions of SR states show large areas of negative values which is a characteristic sign of non-classicality. The photon number distribution and Wigner function of the SR state are found to be very similar to those of the DFS $|\alpha, k\rangle$ with $k = 1$. The overlap between the Wigner functions of the experimental SR state and DFS gives the fidelity value of 0.72.

One of the features of DFS is that the state is determined by its photon number while the phase is completely random [13]. This fact can explain abnormally large phase fluctuations of the SR emission

which have been previously observed [36]. The physical reason why the observed SR states look very similar to DFS and whether they are actual DFS is unclear at the moment and requires an additional study. Finally, the present optical quantum technologies operate with either c.w. emission or long (microsecond–millisecond) pulses at relatively low repetition rates. The advantages of the femtosecond quantum light are presently unclear. We hope that future developments of quantum technologies will require advantages provided by femtosecond optical pulses.

Acknowledgments

The authors would like to thank I H White for support, H Kan and H Ohta for the fabrication of the heterostructures, and V I Man'ko for fruitful discussions and helpful comments. The authors acknowledge the funding from EPSRC (Grant # EP/M013472/1).

References

[1] Schleich W 2001 *Quantum Optics in Phase Space* (Berlin: Wiley)
[2] Walmsley I A 2015 *Science* **348** 525–30
[3] Browne D, Bose S, Mintert F and Kim M S 2017 *Prog. Quant. Electron.* **54** 2
[4] Dodonov V V 2002 *J. Opt.* **4** R1
[5] Schleich W and Wheeler J A 1987 *Nature* **326** 574
[6] Mandel L 1979 *Opt. Lett.* **4** 205
[7] Stoler D 1974 *Phys. Rev. Lett.* **33** 1397
[8] Nielsen M A and Chuang I L 2000 *Quantum Computation and Quantum Information* (Cambridge: Cambridge University Press)
[9] Schleich W, Pernigo M and Kien F L 1991 *Phys. Rev.* A **44** 2172
[10] Buzek V, Vidiella-Barranco A and Knight P L 1992 *Phys. Rev.* A **45** 6570
[11] Glauber R J 2007 *Ann. Phys.* **16** 6
[12] Buzek V and Knight P L 1995 *Prog. Optic.* **34** 1
[13] de Oliveira F A M, Kim M S, Knight P L and Buzek V 1990 *Phys. Rev.* A **41** 2645
[14] Wolfe E and Yelin S F 2014 *Phys. Rev. Lett.* **112** 140402
[15] Aparicio Alcalde M, Cardenas A H, Svaiter N F and Bezerra V B 2010 *Phys. Rev.* A **81** 032335
[16] Ficeka Z and Tana R 2002 *Phys. Rep.* **372** 369
[17] Bhatti D, von Zanthier J and Agarwal G S 2015 *Sci. Rep.* **5** 17335
[18] Dicke R H 1954 *Phys. Rev.* **93** 99
[19] Garraway B M 2011 *Phil. Trans. R. Soc.* A **369** 1137
[20] Baumann K, Guerlin C, Brennecke F and Esslinger T 2010 *Nature* **464** 1301
[21] Kirton P and Keeling J 2018 *New J. Phys.* **20** 015009
[22] Scheibner M, Schmidt T, Worschech L, Forchel A and Bacher G 2007 *Nat. Phys.* **3** 106
[23] Vasil'ev P P 2009 *Rep. Prog. Phys.* **72** 076501
[24] Vasil'ev P P, Olle V, Penty R V and White I H 2013 *Europhys. Lett.* **104** 40003
[25] Vasil'ev P P, Penty R V and White I H 2016 *Light Sci. Appl.* **5** e16086
[26] Vasil'ev P P, Penty R V and White I H 2018 *Opt. Exp.* **26** 26156
[27] Vasil'ev P P 2004 *Phys. Status Solidi b* **241** 1251
[28] Vasil'ev P P and Smetanin I V 2006 *Phys. Rev.* B **74** 125206
[29] Leonhardt U and Paul H 1995 *Prog. Quant. Electron.* **19** 89
[30] Ourjoumtsev A, Jeong H, Tualle-Brouri R and Grangier P 2007 *Nature* **448** 784
[31] Hacker B, Welte S, Daiss S, Shaukat A, Ritter S, Li L and Rempe G 2019 *Nat. Photon.* **13** 110
[32] Lvovsky A I and Raymer M G 2009 *Rev. Mod. Phys.* **81** 299
[33] Roumpos G and Cundiff S T 2013 *J. Opt. Soc. Am.* B **30** 1303
[34] Esposito M *et al* 2014 *New J. Phys.* **16** 043004
[35] Esposito M *et al* 2016 *EPJ Quantum Technol.* **3** 7
[36] Vasil'ev P P, Olle V, Penty R V and White I H 2013 *Appl. Phys. Lett.* **103** 241108
[37] Mandel L 1986 *Phys. Scr.* T **12** 34
[38] Vasil'ev P 1995 *Ultrafast Diode Lasers: Fundamentals and Applications* (Norwood: Artech House)
[39] Lvovsky A I and Babichev S A 2002 *Phys. Rev.* A **66** 011801
[40] Uhlmann A 1976 *Rep. Math. Phys.* **9** 273
[41] Milburn G L and Walls D F 1988 *Phys. Rev.* A **38** 1087
[42] Marian P, Ghiu I and Marian T A 2013 *Phys. Rev.* A **88** 012316